ASN NEURO RESEARCH ARTICLE

ASN NEURO 2(3):art:e00036.doi:10.1042/AN20100007

Alterations in striatal synaptic transmission are consistent across genetic mouse models of Huntington's disease

Damian M Cummings[1], Carlos Cepeda and Michael S Levine[2]
Intellectual and Developmental Disabilities Research Center, David Geffen School of Medicine, University of California at Los Angeles, Los Angeles, CA 90095, U.S.A.

Cite this article as: Cummings DM, Cepeda C and Levine MS (2010) Alterations in striatal synaptic transmission are consistent across genetic mouse models of Huntington's disease. ASN NEURO 2(3):art:e00036.doi:10.1042/AN20100007

ABSTRACT

Since the identification of the gene responsible for HD (Huntington's disease), many genetic mouse models have been generated. Each employs a unique approach for delivery of the mutated gene and has a different CAG repeat length and background strain. The resultant diversity in the genetic context and phenotypes of these models has led to extensive debate regarding the relevance of each model to the human disorder. Here, we compare and contrast the striatal synaptic phenotypes of two models of HD, namely the YAC128 mouse, which carries the full-length huntingtin gene on a yeast artificial chromosome, and the CAG140 KI (knock-in) mouse, which carries a human/mouse chimaeric gene that is expressed in the context of the mouse genome, with our previously published data obtained from the R6/2 mouse, which is transgenic for exon 1 mutant huntingtin. We show that striatal MSNs (medium-sized spiny neurons) in YAC128 and CAG140 KI mice have similar electrophysiological phenotypes to that of the R6/2 mouse. These include a progressive increase in membrane input resistance, a reduction in membrane capacitance, a lower frequency of spontaneous excitatory postsynaptic currents and a greater frequency of spontaneous inhibitory postsynaptic currents in a subpopulation of striatal neurons. Thus, despite differences in the context of the inserted gene between these three models of HD, the primary electrophysiological changes observed in striatal MSNs are consistent. The outcomes suggest that the changes are due to the expression of mutant huntingtin and such alterations can be extended to the human condition.

Key words: CAG 140 knock-in mouse model, electrophysiology, Huntington's disease, striatum, YAC128 mouse model.

INTRODUCTION

Since the identification of the *huntingtin* gene (The Huntington's Disease Collaborative Research Group, 1993), many genetic models of HD (Huntington's disease) have been generated, ranging from transfected cells to invertebrates, rodents and, most recently, primates. The most studied of these are the mouse models of HD, which have been shown to replicate facets of the disorder (Bates et al., 2002; Hickey and Chesselet, 2003; Levine et al., 2004). Mouse models have employed a number of different approaches for delivery of the mutant gene and a range of promoters to drive expression at various levels. In addition, experimenters have used either truncated or full-length DNA. The differences in genetic context and resultant phenotypes of these models have led to extensive debate regarding the consistency of outcomes and relevance to the human disorder. Often different research groups have chosen a preferred model in which to conduct experiments, and findings from different models are not systematically contrasted. In a comparative study, we recently reported that similar electrophysiological synaptic phenotypes were identifiable in cortical pyramidal neurons of three different mouse models of HD (Cummings et al., 2009). The first was the R6/2, the most widely studied mouse model of HD (Bates and Hockly, 2003; Woodman et al.,

[1] Present address: Department of Neuroscience, Physiology and Pharmacology, University College London, Gower Street, London WC1E 6BT, U.K.
[2] To whom correspondence should be addressed (email mlevine@mednet.ucla.edu).
Abbreviations: ACSF, artificial cerebrospinal fluid; AP5, DL-2-amino-5-phosphonovaleric acid; BIC, bicuculline methobromide; CNQX, 6-cyano-7-nitroquinoxaline-2,3-dione; EPSC, excitatory postsynaptic current; $GABA_A$, γ-aminobutyric acid type A; HF, high frequency; HD, Huntington's disease; IPSC, inhibitory postsynaptic current; KI, knock-in; LF, low frequency; MSN, medium-sized spiny neuron; WT, wild-type.

2007), which expresses a truncated transgene consisting of exon 1 with ~150 CAG repeats (Mangiarini et al., 1996). The second, the YAC128 mouse, carries the full-length HD gene on a yeast artificial chromosome (Slow et al., 2003). The third model used a gene-targeting or KI (knock-in) approach to insert a chimaeric mouse/human exon 1 containing 140 CAG repeats into the murine *huntingtin* homologue (*Hdh*) and thus expresses the mutant HD gene in the normal context of the mouse genome (Menalled et al., 2003). We concluded that the basic cortical electrophysiological phenotype is consistent across these models and is likely to be true for the human disease.

In the present experiments, we compared electrophysiological alterations in synaptic transmission in striatal MSNs (medium-sized spiny neurons) in the same three models. Previously, we described progressive decreases in the frequency of spontaneous EPSCs (excitatory postsynaptic currents) and increases in spontaneous IPSCs (inhibitory postsynaptic currents) in MSNs of both R6/2 and R6/1 mice (Cepeda et al., 2003, 2004). Here, we examined spontaneous EPSCs and IPSCs in MSNs in the YAC128 and CAG140 KI mice. We demonstrate that the progressive decrease in excitation and increase in inhibition also occur in these mouse models and therefore likely represent a striatal synaptic dysfunction in human HD.

MATERIALS AND METHODS

Animals

Mice were obtained from our colonies at the UCLA (University of California Los Angeles). All procedures were performed in accordance with the *USPHS Guide for Care and Use of Laboratory Animals* and were approved by the Institutional Animal Care and Use Committee at UCLA. Transgenic mice containing the full-length human HD gene with 128 CAG repeats on a yeast artificial chromosome (YAC128, line 53) (Slow et al., 2003), maintained on an FVB/N background, were examined at 1, 6 and 12 months of age. KI mice had a chimaeric mouse/human exon 1 containing 140 CAG repeats inserted into the murine *huntingtin* gene (Menalled et al., 2003), maintained on a mixed 129/SVXC57BL/6 background, were examined at 6, 12 and 18 months of age. These ages were based on previous studies defining behavioural phenotypic milestones in each of the lines (Slow et al., 2003; Hickey et al., 2008). Appropriate age-matched WT (wild-type) littermates were used as controls. Mice were genotyped at least twice, once at weaning and again after experimentation, to verify genotype. For all experiments, mice of both genders were used as there were no consistent differences between measures obtained from males and females.

Slice preparation

Mice were anaesthetized using halothane and then decapitated, and the brain rapidly removed to ice-cold dissection ACSF (artificial cerebrospinal fluid), containing 130 mM NaCl, 3 mM KCl, 26 mM $NaHCO_3$, 1.25 mM $NaHPO_4$, 10 mM glucose, 5 mM $MgCl_2$ and 1 mM $CaCl_2$; aerated with 95% O_2/5% CO_2; pH=7.2; 290–300 mOsm/l. The hindbrain was removed with a razor blade and glued by the caudal axis to the stage of a vibrating microtome (model VT1000S; Leica), and 350 μm coronal slices that included the striatum were cut. Slices were then stored and allowed to recover at room temperature (25°C) in a submerged chamber in oxygenated standard ACSF (the same composition as dissection ACSF, except that $MgCl_2$ and $CaCl_2$ were 2 mM) for at least 1 h prior to experimentation.

Whole-cell patch–clamp recordings

MSNs were visualized in the dorsolateral striatum using IR videomicroscopy and differential interference contrast optics and identified by somatic size and basic membrane properties. Whole-cell patch–clamp recordings were made using glass micropipettes (electrode impedance 4–6 MΩ) filled with a caesium methanesulfonate-based solution containing 125 mM caesium methanesulfonate, 4 mM NaCl, 3 mM KCl, 1 mM $MgCl_2$, 9 mM EGTA, 8 mM Hepes, 5 mM MgATP, 1 mM Tris/GTP, 10 mM disodium phosphocreatine and 0.1 mM leupeptin; pH=7.2; 270–280 mOsm/l. During electrophysiological recordings, slices were continuously perfused in ACSF at a flow rate of ~2 ml/min at room temperature.

To record spontaneous EPSCs and IPSCs, the membrane current was filtered at 1 kHz and digitized at 100–200 μs using Clampex 8.2 (gap-free mode) (Molecular Devices). Cells were voltage-clamped at −70 mV to assess basic membrane properties and to examine glutamate receptor-mediated EPSCs. Where indicated, 20 μM BIC (bicuculline methobromide) was applied in order to block $GABA_A$ (γ-aminobutyric acid type A) receptor-mediated currents. To isolate $GABA_A$ receptor-mediated IPSCs, membranes were stepped to a holding potential of +10 mV and the ionotropic glutamate receptor antagonists CNQX (6-cyano-7-nitroquinoxaline-2,3-dione; 10 μM) and AP5 (DL-2-amino-5-phosphonovaleric acid; 50 μM) were applied. All drugs were obtained from Sigma–Aldrich. Stock solutions were prepared in distilled water (or NaOH for AP5) and then dissolved in ACSF to required concentrations.

Statistical analyses

Spontaneous EPSCs and IPSCs were analysed offline using the automatic detection protocol within MiniAnalysis program (Justin Lee; Synaptosoft; 1999) and subsequently checked manually for accuracy. Event counts were carried out by an experimenter blind to genotype. The threshold amplitude for the detection of an event (5 pA for EPSCs and 10 pA for

IPSCs) was set above the root mean square noise (1–2 pA at $V_{hold}=-70$ mV and 2–4 pA at $V_{hold}=+10$ mV). Event kinetics were analysed using MiniAnalysis software. Events with amplitudes between 10 and 50 pA (EPSCs) and 15 and 70 pA (IPSCs) were aligned by half-rise time and normalized by peak amplitude. Events displaying complex peaks were excluded from this analysis. The decays of both EPSCs and IPSCs could be fitted with second-order exponential curves, and these were used to determine rise time, decay time and half-amplitude durations.

Values in the Figures are presented as means ± S.E.M. Numerical values for the estimated parameters and sample sizes are indicated within the Figures. Differences between group means were assessed with appropriate Student's *t* tests (two-tailed, unpaired with or without Welch's correction for unequal variance) or appropriately designed analyses of variance followed by Bonferroni's post-hoc test. Microsoft Excel and SigmaStat 2.03 (SPSS) were used to perform all statistical analyses.

RESULTS

Basic membrane properties of MSNs

The basic membrane properties of striatal MSNs have been shown to be progressively altered in slices from R6/2 mice (Cepeda et al., 2001, 2004; Klapstein et al., 2001). No differences in input resistance or capacitance in MSNs of R6/2 mice were seen prior to the onset of the overt motor phenotype, while MSNs from behaviourally phenotypic mice showed increased input resistance and decreased capacitance. We therefore assessed basic membrane properties in the YAC128 (Table 1) and CAG140 KI (Table 2) mice. At 1 and 6 months, no differences in the input resistance of YAC128 MSNs and their respective WTs were observed. By 12 months, however, a highly significant ($P<0.0001$) increase in input resistance occurred. No significant differences in membrane capacitance were observed at any age. MSNs from the CAG140 KI mice showed no change in input resistance at 6 months but by 12 ($P<0.01$) and 18 ($P<0.05$) months, MSNs displayed input resistances that were significantly increased compared with their respective WTs. KI mice also showed a decrease in capacitance at 12 ($P<0.05$) and 18 ($P<0.01$) months, but no difference at 6 months.

Spontaneous EPSCs

We next examined spontaneous EPSCs, which have been shown previously to have a progressive decrease in frequency in MSNs of R6/2 and R6/1 mice with overt phenotype progression (Cepeda et al., 2003; Rossi et al., 2006). Similar effects occurred in both the YAC128 and KI models (Figure 1). When cell membranes were voltage-clamped at −70 mV and spontaneous currents recorded in ACSF (Figure 1A, left), YAC128 MSNs at 1 month showed no difference in spontaneous EPSC frequency compared with their WT counterparts. By 6 months, a significant reduction in frequency occurred in YAC128 MSNs ($P=0.01$ compared with WT; $P<0.01$ compared with 1 month YAC128). Further reductions were seen at 12 months ($P<0.001$ compared with WT; $P<0.05$ compared with 6 months YAC128). Similar progressive decreases in EPSC frequency were observed in the CAG140 KI mice (Figure 1A, right). No difference in frequency was observed in CAG140 KI MSNs at 6 months compared with WTs. By 12 months a significant reduction was evident ($P=0.001$ compared with WT; $P<0.001$ compared with 6 months CAG140). This reduction with respect to WTs was maintained at 18 months ($P<0.01$ compared with WT).

Effects of BIC on spontaneous EPSCs

A proportion of the spontaneous currents recorded at −70 mV in standard ACSF could be mediated by $GABA_A$ receptors and/or the excitatory drive of presynaptic cortical and thalamic projection neurons could be suppressed by inhibitory inputs from local interneurons. We applied the $GABA_A$ receptor antagonist BIC (20 μM) to eliminate these influences. Previously, in the R6/2 mice, we observed a reduction of 10–20% in spontaneous EPSC frequency in both genotypes (Cepeda et al., 2003). There was no significant difference in the percentage change seen in WT compared with R6/2 mice and, moreover, the reduction in frequency was maintained. In the YAC128 and KI mice, a different pattern occurred in response to BIC application (Figures 1B and 1C). In all cells from WTs, there was a decrease in frequency of EPSCs in BIC. In YAC128 mice, however, some cells responded with a decrease in frequency, while others responded with an increase (Figures 1B and 1C, left panels). At 1 month, only one of eight cells responded with an increase in frequency after BIC treatment, and the overall outcome of BIC application was not statistically different

Table 1 **Basic membrane properties of MSNs in YAC128 mice**
Sample sizes are indicated in parentheses. Sample means ± S.E.M. are presented. Statistical significance is indicated by ***$P<0.001$.

	1 month		6 months		12 months	
Property	**WT ($n=12$)**	**YAC128 ($n=13$)**	**WT ($n=19$)**	**YAC128 ($n=21$)**	**WT ($n=8$)**	**YAC128 ($n=8$)**
R_m (MΩ)	93.2 ± 13.1	85.1 ± 13.1	89.5 ± 5.3	82.1 ± 5.6	77.3 ± 7.3	147.9 ± 16.6***
τ (ms)	1.5 ± 0.1	1.6 ± 0.1	1.3 ± 0.1	1.7 ± 0.1	1.4 ± 0.1	1.3 ± 0.1
C_m (pF)	79.3 ± 7.8	77.9 ± 5.1	75.1 ± 4.5	79.1 ± 5.0	58.8 ± 4.0	63.6 ± 6.6

Table 2 **Basic membrane properties of MSNs in CAG140 KI mice**
Sample sizes are indicated in parentheses. Sample means ± S.E.M. are presented. Statistical significance is indicated by *$P<0.05$; **$P<0.01$.

	6 months		12 months		18 months	
Property	**WT ($n=7$)**	**KI ($n=11$)**	**WT ($n=16$)**	**KI ($n=35$)**	**WT ($n=7$)**	**KI ($n=11$)**
R_m (MΩ)	88.6 ± 9.2	92.3 ± 13.5	91.1 ± 6.9	137.9 ± 9.5**	87.3 ± 12.5	156.4 ± 20.3*
τ (ms)	1.6 ± 0.1	1.4 ± 0.1	1.6 ± 0.1	1.6 ± 0.1	1.4 ± 0.1	1.6 ± 0.1
C_m (pF)	75.6 ± 7.3	80.0 ± 3.9	84.2 ± 4.1	70.7 ± 3.0*	82.3 ± 4.4	62.5 ± 3.1**

from that of WTs. At 6 months, 36% of cells responded with an increase in EPSC frequency, but the overall outcome of BIC application was still a decrease that was not significantly different from WTs. By 12 months, 75% of cells showed an increase after BIC application and the overall outcome was a significant increase in EPSC frequency ($P<0.001$). Despite the increase in EPSC frequencies in response to BIC, the decrease in spontaneous EPSC frequency in YAC128 mice compared with values in WTs still occurred at 6 and 12 months. At 6 months, the effect was a trend that was not statistically significant ($P=0.07$), but it was significant at 12 months ($P<0.05$).

This differential effect of BIC also occurred in MSNs of CAG140 KI mice (Figures 1B and 1C, right panels). At 6 months, in both WT and KI MSNs, BIC application resulted in a reduction in frequency of EPSCs. At 12 months, 53% of CAG140 KI cells responded with an increase in EPSC frequency and, similarly to the oldest group in the YAC128 mice, the overall effect of BIC did not reach statistical significance ($P=0.06$). Because of the ~25% decrease in frequency seen in WT MSNs and the ~25% increase seen in KI MSNs, the difference in mean EPSC frequency was not maintained in the presence of BIC in this group of cells. Due to the technical difficulties of recording from animals at 18 months of age, the effects of BIC were not tested at this age in the CAG140 KI mice.

Spontaneous IPSCs

We reported previously that two populations of MSNs were identifiable in the R6/2 striatum. One population displayed an LF (low frequency) of IPSCs and was indistinguishable from WTs. The other population displayed an HF (high frequency) of IPSCs, which were never seen in WTs (Cepeda et al., 2004). When IPSCs were isolated at a holding membrane potential of +10 mV in the presence of the ionotropic glutamate receptor antagonists CNQX (10 μM) and AP5 (50 μM), two populations of MSNs were again observed in YAC128 and CAG140 MSNs (Figure 2). At all ages in the YAC128 mice (Figure 2, left), a small population of MSNs with an HF of IPSCs ($P<0.001$ compared with WT) was identified, but only in transgenic mice. Unlike the R6/2, a progressive difference was also observed in the LF population of cells. At 1 month, the mean frequency of LF IPSCs in YAC128 was identical with WTs. At 6 and 12 months, however, there was a significant reduction in frequency in the LF population of cells compared with WTs ($P<0.01$ at both 6 and 12 months).

The changes in IPSCs were less pronounced and transitory in the CAG140 KI mice (Figure 2, right-hand panel). At 6 months, no differences in the frequency of IPSCs, including no cells with HF IPSCs, were observed. At 12 months, both LF and HF cells were identified. Similar to the YAC128 mice, the LF population of cells showed a lower frequency of IPSCs than WTs ($P<0.05$). Very few HF cells were observed (3/18 cells), but these showed a highly significant increase in frequency compared with WTs ($P<0.001$). At 18 months, the LF population of cells maintained a reduction compared with WTs ($P<0.05$), but no HF cells were observed in the cells sampled.

Event kinetics

When the kinetics of averaged spontaneous EPSCs were analysed in R6/2 MSNs, we observed no differences in rise time, decay time or half-amplitude duration for any age (Cepeda et al., 2003). In contrast, Milnerwood and Raymond (2007) demonstrated faster spontaneous EPSC decay kinetics in MSNs of YAC128 mice at 1 month. In our hands, at this age no differences in EPSC kinetics between WT and YAC128 neurons were observed (Figure 3A, left panels). At 6 and 12 months, a faster decay time of EPSCs was observed ($P<0.01$ and $P<0.05$ respectively). Rise time and half-amplitude duration were unaltered at any age. No differences in the EPSC kinetics of 6 or 12 month CAG140 KI mice were identified (Figure 3A, right panels). At 18 months of age, cells from these animals had EPSCs with faster decay times ($P<0.05$).

We also examined the kinetics of spontaneous IPSCs. In the LF and HF populations of R6/2 MSNs, IPSCs were found to have faster decay times (Cepeda et al., 2004) and this effect was also observed in the two lines of mice studied here (Figure 3B). At 1 month of age, IPSCs in the LF population of YAC128 cells (Figure 3B, left panels) had a faster decay time ($P<0.05$). The faster decay time in the HF population of cells did not reach statistical significance. Half-amplitude duration did not show significant differences at this age. By 6 months, both the LF ($P<0.01$) and HF ($P<0.05$) populations had IPSCs with faster decay times and shorter half-amplitude durations, an effect that was maintained at 12 months ($P<0.05$ to $P<0.001$). In the CAG140 KI mice (Figure 3B, right panels), only the HF population of cells at 12 months showed altered IPSC kinetics.

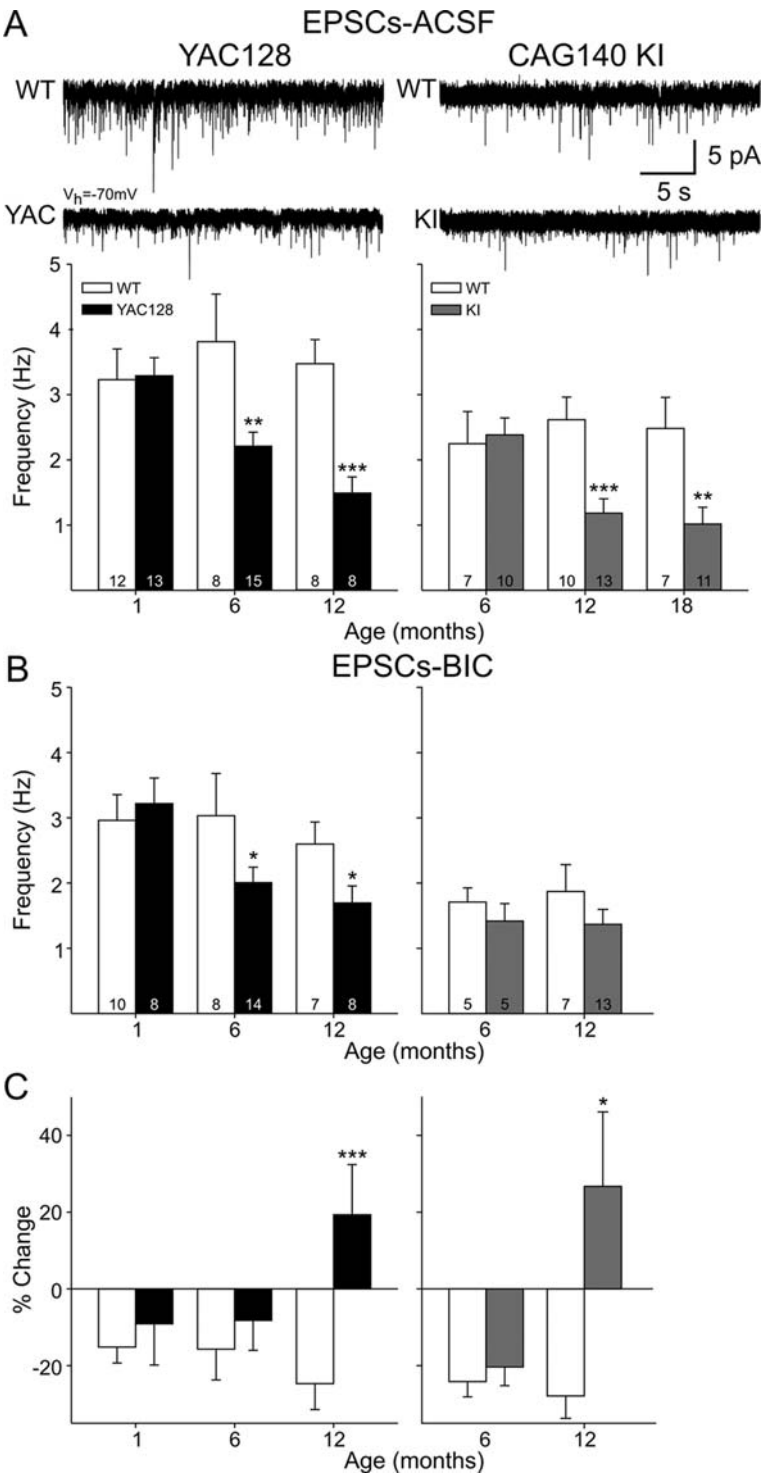

Figure 1 **Spontaneous EPSCs from MSNs of YAC128 and CAG140 KI mice**

(**A**) Typical recordings from 6-month YAC128 and 12-month CAG140 KI mice in ACSF. Mean frequencies ± S.E.M. are plotted for each age. (**B**) Mean frequencies ± S.E.M. for spontaneous EPSCs isolated by BIC. The variation in frequency between the respective WTs at 6 and 12 months is likely due to the difference in background strain. (**C**) Percentage change in EPSC frequency after BIC application. Sample sizes are indicated inside the bars. Sample sizes in (**C**) are the same as (**B**). Statistical significance with respect to WTs is shown by $^{*}P<0.05$, $^{**}P<0.01$ and $^{***}P<0.001$.

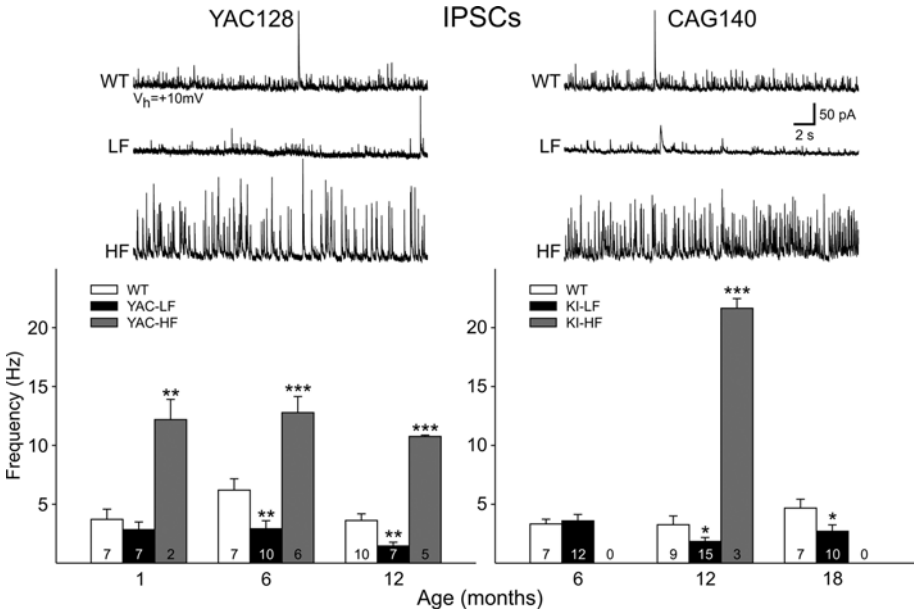

Figure 2 **Spontaneous IPSCs from MSNs of YAC128 and CAG140 KI mice**
Typical recordings from YAC128 at 6 months and CAG140 KI at 12 months. Two populations of cells were identified in mutant animals only. One displayed LF IPSCs and the other HF IPSCs. IPSCs were isolated at a holding potential of +10 mV and in the presence of CNQX and AP5. Results show mean frequencies ± S.E.M. for each age. Statistical significance with respect to WTs is indicated by $^{**}P<0.01$ and $^{***}P<0.001$.

In this group of cells, both decay time and half-amplitude duration were reduced ($P<0.05$).

DISCUSSION

The present experiments demonstrate that both YAC128 and CAG140 KI mouse models of HD show similar alterations in basic membrane properties and both spontaneous EPSCs and IPSCs to those observed previously in the R6/2 and R6/1 models of HD (Cepeda et al., 2003, 2004; Cummings et al., 2009). The reduction in EPSC frequency has also been confirmed by others in the R6/2 mouse and the neurotoxic 3-nitropropionic acid rat model of HD (Rossi et al., 2006). Spontaneous EPSCs were also studied by Milnerwood and Raymond (2007) in MSNs of the YAC128 mouse at 1 month of age and, similar to our results, no differences in EPSC frequency were identified, although there were changes in EPSC kinetics. Here, we extend the striatal data in YAC128 to 12 months and CAG140 KI mice to 18 months, demonstrating a reduction in EPSC frequency. Similarly, a reduction in spontaneous EPSCs has been observed at 6 months in a model of HD in which full-length human huntingtin is carried on a bacterial artificial chromosome with 97 mixed CAA-CAG repeats (Gray et al., 2008). Similar to the present dataset, the cortical electrophysiological phenotype was demonstrated to be common to each of the R6/2, YAC128 and CAG140 KI mouse models of HD (Cummings et al., 2009).

MSNs receive a major excitatory drive from the cortex, in which pyramidal neurons from almost the whole cortical mantle, but in particular the motor and somatosensory cortices, project to the striatum (Bolam et al., 2000). Therefore the reduction in EPSC frequency probably represents a disconnection between the cortex and striatum, which is likely to be mediated by the loss of spines and the presence of dysmorphic neuronal processes characteristic of both cortical and striatal neurons in HD (Klapstein et al., 2001). Thalamostriatal projections also provide an excitatory input on to MSNs (Ding et al., 2008; Smeal et al., 2008). Corticostriatal and thalamostriatal terminals appear to be equal in number in non-disease states (Lacey et al., 2005) and may synapse on to distinct populations of MSNs (Dubé et al., 1988) and excitatory synapses formed by corticostriatal and thalamostriatal projections have differential electrophysiological properties (Ding et al., 2008; Smeal et al., 2008). However, the properties of neurons within the thalamic nuclei or their influences on striatal neurons have yet to be determined in HD.

There were commonalities and differences in GABAergic neurotransmission between the three models of HD. All showed two populations of cells, one with LF IPSCs and one with HF IPSCs. No difference was observed between the LF IPSCs in the R6/2 mouse compared with WTs (Cepeda et al., 2004). In contrast, in both the YAC128 and CAG140 KI mice there were reductions in frequency compared with their respective WTs for this population of cells. Whereas the change in glutamatergic neurotransmission probably reflects alterations in corticostriatal (and thalamostriatal) connections,

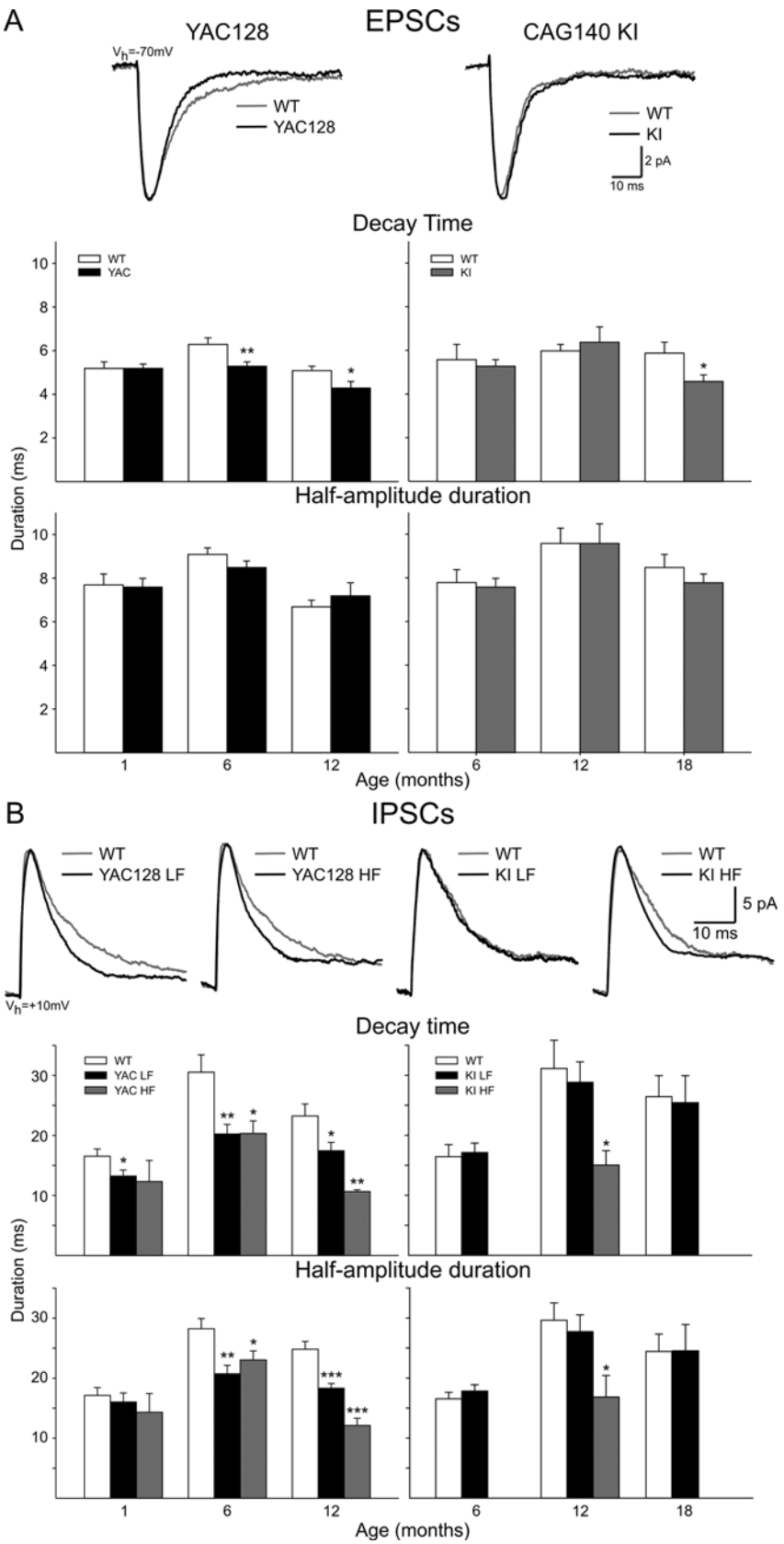

Figure 3 **Decay kinetics of spontaneous postsynaptic currents in MSNs of YAC128 and CAG140 KI mice**
(**A**) Top: examples of averaged spontaneous EPSCs from WT (grey) and mutant (black) mice (YAC128, 6 months; CAG140 KI, 12 months). Middle: means ± S.E.M. of decay times for each age. Bottom: means ± S.E.M. of half-amplitude durations for each age. (**B**) Top: examples of averaged spontaneous IPSCs from WT (grey) and mutant (black) mice (YAC128, 6 months; CAG140 KI, 12 months). Middle: means ± S.E.M. of decay times for each age. Bottom: means ± S.E.M. of half-amplitude durations for each age. Sample sizes are shown in Figure 1(A) for EPSCs and Figure 2 for IPSCs. Statistical significance is indicated by $*P<0.05$, $**P<0.01$ and $***P<0.001$ with respect to WT.

the alterations in GABAergic currents reflect abnormal synaptic transmission local to the striatum. MSNs receive a major inhibitory drive from striatal interneurons (Tepper et al., 2004, 2008; Plotkin et al., 2005) and it is therefore likely that dysfunctional, fast-spiking GABAergic interneurons underlie the changes observed in inhibitory currents in MSNs. Altered MSN–MSN interactions may also be of importance, as these neurons receive inputs from other MSNs via both electrical (gap junction) and chemical (synaptic) connections (Wilson and Groves, 1980; Venance et al., 2004), although their importance relative to fast-spiking interneuronal inputs is still debated (Tunstall et al., 2002; Czubayko and Plenz, 2002). Furthermore, connectivity between interneurons has been shown to affect both excitatory and inhibitory inputs to MSNs, as knockout of the neuronal gap junction gene for connexin 36 leads to reductions in both EPSC and IPSC frequency (Cummings et al., 2008). An altered connexin 43 expression pattern has been demonstrated in post-mortem HD brain (Vis et al., 1998). While the connexin 43 subunit is associated with the coupling of astrocytes, if changes in the neuronal connexin

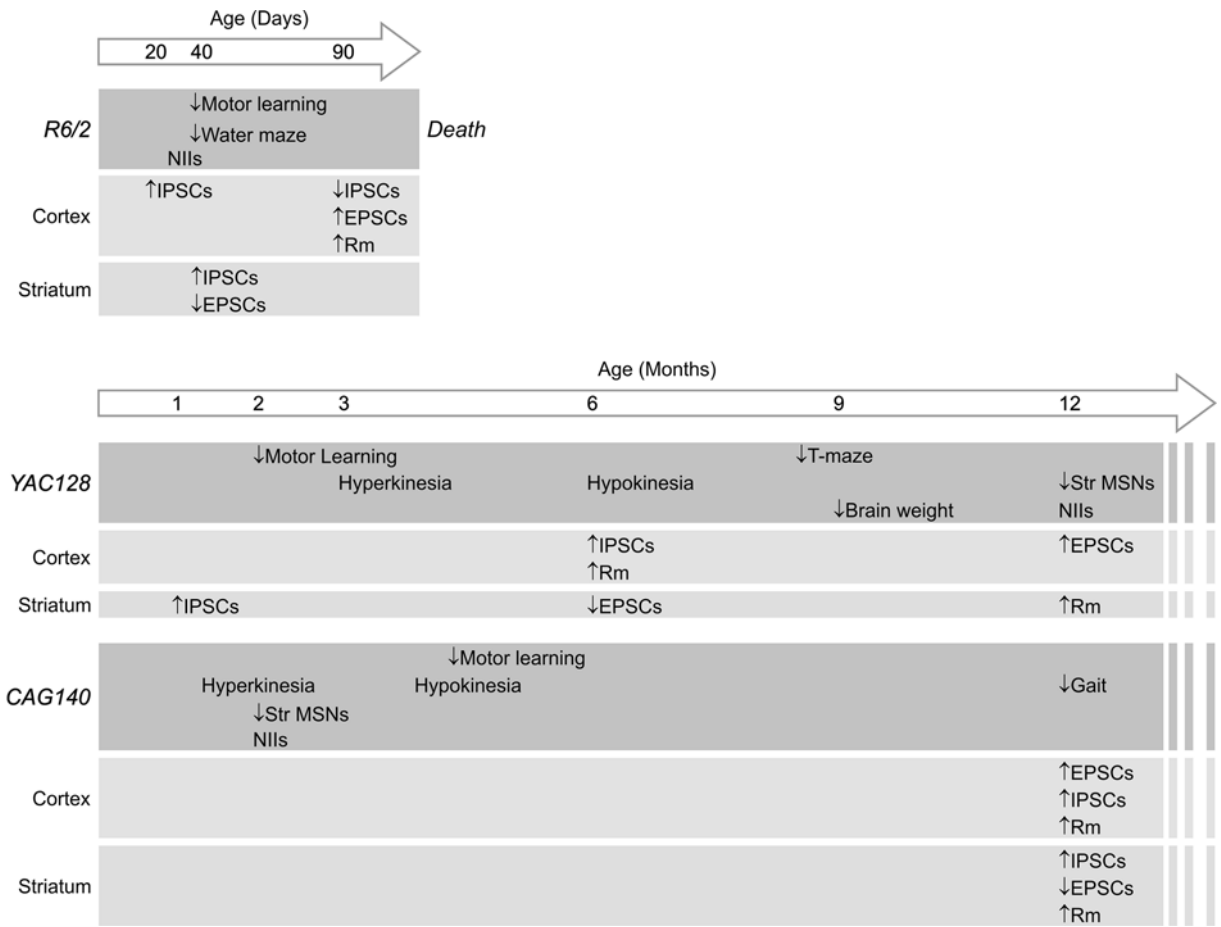

Figure 4 **Timeline of key phenotypes including striatal and cortical electrophysiology**
Age in days and months are indicated within the arrows. Each phenotype is indicated such that the labels begin at the earliest age detected. Timelines are shown for R6/2 (top), YAC128 (middle) and CAG140 KI (bottom) with key behavioural, cognitive and morphological phenotypes (green bars), as well as cortical (beige bars) and striatal (blue bars) electrophysiological phenotypes. Upward arrows indicate increases or improvements; downward arrows indicate decreases or deficits. Electrophysiological striatal and cortical phenotypes are summarized from the present paper and from Cummings et al. (2009) and Cepeda et al. (2003, 2004). Behavioural, cognitive and morphological phenotypes are from Lione et al. (1999), Meade et al. (2002), Hickey et al. (2008), Menalled et al. (2003), Van Raamsdonk et al. (2005) and Slow et al. (2003).

36 occur in HD, altered interneuronal synchrony is likely to result.

The influence of $GABA_A$ receptor-mediated inhibition on EPSCs was altered differentially in the YAC128 and CAG140 mice, a finding contrary to that in the R6/2 mouse model (Cepeda et al., 2003). In R6/2 (and WT) mice, application of a $GABA_A$ receptor antagonist reduced the frequency of events recorded at a holding potential of −70 mV, suggesting that a proportion of these events were GABAergic in origin. In contrast, in MSNs from YAC128, a higher proportion of cells responded with an increase in frequency upon $GABA_A$ receptor blockade as animals aged. This was also observed at 12 months in MSNs from CAG140 KIs. Such an effect may be due to altered inhibition within the striatum, which may be shunting excitatory inputs received from the cortical and thalamic terminals. Alternatively, cortical pyramidal cells are known to be hyperexcitable in the R6/2, YAC128 and CAG140 KI models of HD (Walker et al., 2008; Cummings et al., 2009). Application of BIC to the corticostriatal slices may thus exacerbate the hyperexcitability of cortical cells, leading to increased release of glutamate, reflected in MSNs as increased EPSC frequency.

The rate of progression of the electrophysiological phenotypes varied between the different models (Figure 4). This divergence is likely to be due to a combination of the precise regulation of the huntingtin gene expressed in the alternative models and cumulative compensatory mechanisms, which may be more prevalent in the slower onset models. Differences in EPSC frequency were detectable as early as 40 days in the R6/2 model, while no differences were detected until 6 months in the YAC128 and only at 1 year in the CAG140 KI. These effects correspond to previous reports of phenotypic progression in the YAC128 and KI lines. The finding that no difference in EPSC frequency was observed at the youngest ages in any line of HD mouse models suggests that presymptomatic HD gene carriers are likely to have more normal excitatory inputs to MSNs. In contrast, IPSC frequency increased in a population of cells in the youngest age group of YAC128 mice and a trend towards an increase in IPSC frequency was evident in R6/2 mice (Cepeda et al., 2004), but no difference was observed in CAG140 mice. This suggests that alterations in inhibitory inputs probably from fast-spiking interneurons within the striatum are affected at a much earlier stage than the excitatory inputs received by MSNs from cortical and thalamic projections. Furthermore, our previous data suggest that a cortical electrophysiological dysfunction may occur earlier than observed in the striatum and that the predominant cortical phenotype is an alteration in GABAergic neurotransmission (Cummings et al., 2009). As interneurons are relatively spared in HD (Ferrante et al., 1985), there has yet to be a systematic electrophysiological examination of striatal interneurons in an HD mouse model to determine whether and how they are dysfunctional.

The differences that we identified between the models included altered EPSC kinetics, an altered effect of $GABA_A$ receptor blockade on EPSC frequency, and a reduced frequency of IPSCs in a subpopulation of cells in YAC128 and CAG140 KI mice that were not observed in R6/2 mice. These differences may suggest that these alterations require the full-length mutant huntingtin to occur or may reflect the presence of the transgene over a protracted period of time and would therefore not be observed in the R6/2 mouse that reaches end stage at approx. 3–4 months of age. It is tempting to speculate, therefore, that the disparate finding observed in R6/2, YAC128 and CAG140 mice may represent differences between adult- and juvenile-onset HD. Notwithstanding these differences, the predominant synaptic phenotype was consistently observed across models. Recently, an *in vivo* study of striatal MSNs showed reduced bursts of HF activity and a loss of synchrony in both the R6/2 and CAG140 KI mice (Miller et al., 2008). Also, the R6/2 mouse and a KI mouse carrying 150 CAG repeats showed consistent changes in molecular phenotypes when background strain and disease progression were taken into account (Woodman et al., 2007). Therefore it appears that the precise HD gene construct does not significantly alter the basic electrophysiological phenotypes observed in the cortex (Cummings et al., 2009) and striatum.

In conclusion, we demonstrate that a full-length model (YAC128) and a targeted model (CAG140 KI) of HD display similar basic striatal electrophysiological phenotypes to the R6/2 mouse, namely a decrease in EPSC and an increase in IPSC frequencies in striatal MSNs. The consistency of these phenotypes across different mouse models of HD suggests that these changes are a result of the mutant huntingtin gene rather than being idiosyncratic to a particular model.

ACKNOWLEDGEMENTS

We thank Michael Yim and Bianca Marcolino for their help with data analysis and Donna Crandall for preparing the Figures.

FUNDING

This work was supported by the National Institutes of Health [grant number USPHS NS41574] and the Cure Huntington's Disease Initiative, Inc.

REFERENCES

Bates G, Harper PS, Jones L (2002) Huntington's Disease, 3rd edn, Oxford University Press, Oxford and New York.

Bates GP, Hockly E (2003) Experimental therapeutics in Huntington's disease: are models useful for therapeutic trials? Curr Opin Neurol 16:465–470.

Bolam JP, Hanley JJ, Booth PA, Bevan MD (2000) Synaptic organisation of the basal ganglia. J Anat 196:527–542.

Cepeda C, Ariano MA, Calvert CR, Flores-Hernandez J, Chandler SH, Leavitt BR, Hayden MR, Levine MS (2001) NMDA receptor function in mouse models of Huntington disease. J Neurosci Res 66:525–539.

Cepeda C, Hurst RS, Calvert CR, Hernandez-Echeagaray E, Nguyen OK, Jocoy E, Christian LJ, Ariano MA, Levine MS (2003) Transient and progressive electrophysiological alterations in the corticostriatal pathway in a mouse model of Huntington's disease. J Neurosci 23:961–969.

Cepeda C, Starling AJ, Wu N, Nguyen OK, Uzgil B, Soda T, André VM, Ariano MA, Levine MS (2004) Increased GABAergic function in mouse models of Huntington's disease: reversal by BDNF. J Neurosci Res 78:855–867.

Cummings DM, Yamazaki I, Cepeda C, Paul DL, Levine MS (2008) Neuronal coupling via connexin36 contributes to spontaneous synaptic currents of striatal medium-sized spiny neurons. J Neurosci Res 86:2147–2158.

Cummings DM, Andre VM, Uzgil BO, Gee SM, Fisher YE, Cepeda C, Levine MS (2009) Alterations in cortical excitation and inhibition in genetic mouse models of Huntington's disease. J Neurosci 29:10371–10386.

Czubayko U, Plenz D (2002) Fast synaptic transmission between striatal spiny projection neurons. Proc Natl Acad Sci USA 99:15764–15769.

Ding J, Peterson JD, Surmeier DJ (2008) Corticostriatal and thalamostriatal synapses have distinctive properties. J Neurosci 28:6483–6492.

Dubé L, Smith AD, Bolam JP (1988) Identification of synaptic terminals of thalamic or cortical origin in contact with distinct medium-size spiny neurons in the rat neostriatum. J Comp Neurol 267:455–471.

Ferrante RJ, Kowall NW, Beal MF, Richardson Jr EP, Bird ED, Martin JB (1985) Selective sparing of a class of striatal neurons in Huntington's disease. Science 230:561–563.

Gray M, Shirasaki DI, Cepeda C, Andre VM, Wilburn B, Lu XH, Tao J, Yamazaki I, Li SH, Sun YE, Li XJ, Levine MS, Yang XW (2008) Full-length human mutant huntingtin with a stable polyglutamine repeat can elicit progressive and selective neuropathogenesis in BACHD mice. J Neurosci 28:6182–6195.

Hickey MA, Chesselet MF (2003) The use of transgenic and knock-in mice to study Huntington's disease. Cytogenet Genome Res 100:276–286.

Hickey MA, Kosmalska A, Enayati J, Cohen R, Zeitlin S, Levine MS, Chesselet MF (2008) Extensive early motor and non-motor behavioral deficits are followed by striatal neuronal loss in knock-in Huntington's disease mice. Neuroscience 157:280–295.

Klapstein GJ, Fisher RS, Zanjani H, Cepeda C, Jokel ES, Chesselet MF, Levine MS (2001) Electrophysiological and morphological changes in striatal spiny neurons in R6/2 Huntington's disease transgenic mice. J Neurophysiol 86:2667–2677.

Lacey CJ, Boyes J, Gerlach O, Chen L, Magill PJ, Bolam JP (2005) GABA(B) receptors at glutamatergic synapses in the rat striatum. Neuroscience 136:1083–1095.

Levine MS, Cepeda C, Hickey MA, Fleming SM, Chesselet MF (2004) Genetic mouse models of Huntington's and Parkinson's diseases: illuminating but imperfect. Trends Neurosci 27:691–697.

Lione LA, Carter RJ, Hunt MJ, Bates GP, Morton AJ, Dunnett SB (1999) Selective discrimination learning impairments in mice expressing the human Huntington's disease mutation. J Neurosci 19:10428–10437.

Mangiarini L, Sathasivam K, Seller M, Cozens B, Harper A, Hetherington C, Lawton M, Trottier Y, Lehrach H, Davies SW, Bates GP (1996) Exon 1 of the HD gene with an expanded CAG repeat is sufficient to cause a progressive neurological phenotype in transgenic mice. Cell 87:493–506.

Meade CA, Deng YP, Fusco FR, Del Mar N, Hersch S, Goldowitz D, Reiner A (2002) Cellular localization and development of neuronal intranuclear inclusions in striatal and cortical neurons in R6/2 transgenic mice. J Comp Neurol 449:241–269.

Menalled LB, Sison JD, Dragatsis I, Zeitlin S, Chesselet MF (2003) Time course of early motor and neuropathological anomalies in a knock-in mouse model of Huntington's disease with 140 CAG repeats. J Comp Neurol 465:11–26.

Miller BR, Walker AG, Shah AS, Barton SJ, Rebec GV (2008) Dysregulated information processing by medium spiny neurons in striatum of freely behaving mouse models of Huntington's disease. J Neurophysiol 100:2205–2216.

Milnerwood AJ, Raymond LA (2007) Corticostriatal synaptic function in mouse models of Huntington's disease: early effects of huntingtin repeat length and protein load. J Physiol 585:817–831.

Plotkin JL, Wu N, Chesselet MF, Levine MS (2005) Functional and molecular development of striatal fast-spiking GABAergic interneurons and their cortical inputs. Eur J Neurosci 22:1097–1108.

Rossi S, Prosperetti C, Picconi B, De Chiara V, Mataluni G, Bernardi G, Calabresi P, Centonze D (2006) Deficits of glutamate transmission in the striatum of toxic and genetic models of Huntington's disease. Neurosci Lett 410:6–10.

Slow EJ, van Raamsdonk J, Rogers D, Coleman SH, Graham RK, Deng Y, Oh R, Bissada N, Hossain SM, Yang YZ, Li XJ, Simpson EM, Gutekunst CA, Leavitt BR, Hayden MR (2003) Selective striatal neuronal loss in a YAC128 mouse model of Huntington disease. Hum Mol Genet 12:1555–1567.

Smeal RM, Keefe KA, Wilcox KS (2008) Differences in excitatory transmission between thalamic and cortical afferents to single spiny efferent neurons of rat dorsal striatum. Eur J Neurosci 28:2041–2052.

Tepper JM, Koos T, Wilson CJ (2004) GABAergic microcircuits in the neostriatum. Trends Neurosci 27:662–669.

Tepper JM, Wilson CJ, Koos T (2008) Feedforward and feedback inhibition in neostriatal GABAergic spiny neurons. Brain Res Rev 58:272–281.

The Huntington's Disease Collaborative Research Group (1993) A novel gene containing a trinucleotide repeat that is expanded and unstable on Huntington's disease chromosomes. Cell 72:971–983.

Tunstall MJ, Oorschot DE, Kean A, Wickens JR (2002) Inhibitory interactions between spiny projection neurons in the rat striatum. J Neurophysiol 88:1263–1269.

Van Raamsdonk JM, Murphy Z, Slow EJ, Leavitt BR, Hayden MR (2005) Selective degeneration and nuclear localization of mutant huntingtin in the YAC128 mouse model of Huntington disease. Hum Mol Genet 14:3823–3835.

Venance L, Glowinski J, Giaume C (2004) Electrical and chemical transmission between striatal GABAergic output neurones in rat brain slices. J Physiol 559:215–230.

Vis JC, Nicholson LF, Faull RL, Evans WH, Severs NJ, Green CR (1998) Connexin expression in Huntington's diseased human brain. Cell Biol Int 22:837–847.

Walker AG, Miller BR, Fritsch JN, Barton SJ, Rebec GV (2008) Altered information processing in the prefrontal cortex of Huntington's disease mouse models. J Neurosci 28:8973–8982.

Wilson CJ, Groves PM (1980) Fine structure and synaptic connections of the common spiny neuron of the rat neostriatum: a study employing intracellular inject of horseradish peroxidase. J Comp Neurol 194:599–615.

Woodman B, Butler R, Landles C, Lupton MK, Tse J, Hockly E, Moffitt H, Sathasivam K, Bates GP (2007) The Hdh (Q150/Q150) knock-in mouse model of HD and the R6/2 exon 1 model develop comparable and widespread molecular phenotypes. Brain Res Bull 72:83–97.

Received 26 February 2010/23 April 2010; accepted 5 May 2010

Published as Immediate Publication 18 May 2010, doi 10.1042/AN20100007